Zhongfeng Zhang
Qingwen Xue
Lixia Wen
Weihua Peng
Han Shao
Wenzhi Fu ✉

https://doi.org/10.21278/TOF.472051222
ISSN 1333-1124
eISSN 1849-1391

STUDY ON MULTI-STEP FORMING PATHS FOR DOUBLE CURVED PARTS OF 1561 ALUMINIUM ALLOY

Summary

Recently, corrosion-resistant 1561 aluminium alloy has been widely applied to the production of curved parts. However, the sheets of this material will generate a high amount of springback during multi-point forming, which means that a large amount of springback compensation is required. In this paper, four multi-step forming paths are designed to study the effect of forming paths on the multi-point forming results of double curved parts for 1561 aluminium alloy. Numerical simulation of the multi-step forming of curved sheets is carried out by ABAQUS finite element simulation software. The simulation results indicate that the 1561 aluminium alloy double curved parts produce poor situations such as wrinkling and low forming accuracy in single-step forming, while the accuracy improves significantly and the forming quality increases after four-step forming. Therefore, a four-step forming path was adopted for stamping tests on double curved parts. The results of the accuracy inspection of the formed parts by Gom-inspect demonstrate that the quality of the curved parts can be effectively improved by four-step forming, which has a certain significance in guiding the forming preparation of parts for engineering applications.

Key words: *1561 aluminium alloy, multi-step forming, multi-step forming, springback compensation, numerical simulation*

1. Introduction

Most of the outer plates of ships are curved parts with different shapes, and the traditional integral die is only suitable for stamping and forming single-shaped parts, so it is necessary to replace several sets of dies to meet production demand [1], which has a high preparation cost and low production efficiency. Multi-point forming is a flexible, dieless forming technology that uses groups of independent [2] height-adjustable punches instead of integral die, allowing the stamping and forming of a wide range of curved parts with high versatility. 1561 aluminium alloy, as an excellent corrosion-resistant alloy, is widely used in ship manufacturing [3]. Due to the high springback of this material, the deformation required for curved parts increases significantly, resulting in wrinkles and straight edges on the surface of the parts [4,5]. For parts

requiring large deformation, a multi-step, multi-point forming procedure can be used to reduce the amount of single deformation, which can make the forming process easier and improve its quality, and is an effective solution for the wrinkling of curved parts [6-8].

Multi-point forming has been widely used as a forming method for sheets. Sun studied the factors affecting the amount of springback in the multi-point forming of sheets and found that increasing the thickness of the sheet could reduce the springback [9]. Li et al. studied the springback prediction method for anisotropic materials based on the crystal plasticity theory [10]; Zhang studied the springback compensation algorithm for elastic-plastic materials with single surfaces [11].

As an extended application of multi-step forming, multi-step forming of thin plates has been investigated by using the finite element method [12].

(1) About spherical parts:

To solve the problem of the edge wrinkling of spherical parts formed in one step, Hao used the multi-step forming method and found that the number of steps needed to form decreased as the thickness of the part increased [13]. Qian et al. investigated the effect of elastic pad thickness on the quality of the multi-step forming of aluminium alloy spherical parts and found that an elastic pad with reasonable thickness can effectively reduce part indentation and improve the dimensional accuracy of the formed parts [14].

(2) About saddle surface parts:

Liu et al. compared the forming state of saddle parts after single and multiple steps, and then found that the multiple steps forming process could significantly alleviate wrinkling in the central area of the part and improve the forming quality of the saddle parts [15]. Liu Wei also pointed out in a study of the multi-step forming of saddle parts that the forming accuracy of the saddle parts is improved due to the increase in the amount of multi-step forming and the reduction of single-step deformation [16].

Currently, most applications of multi-step forming focus on symmetrical, regular surface parts such as spherical and saddle parts, while any investigation of asymmetrical surface parts is rare. In this paper, a multi-step, multi-point forming process is investigated for asymmetric double curved parts. The simulation analysis of the forming process is carried out by finite element simulation with ABAQUS. By comparing the effects of different forming paths on the accuracy of the formed parts, the multi-step forming paths are optimized. The effect of multi-step forming on the straight edge effect is studied, and the simulation results are verified experimentally to provide useful guidance for production practice.

2. Materials experiment

The chemical composition of 1561 aluminium alloy plate (density of 2.7 g/cm^{-3}) is shown in Table 1.

Table 1 Chemical composition of 1561 aluminium (wt.-%)

Mg	Mn	Fe	Si	Zn	Zr	Cu	Al
6.2	0.85	0.4	0.4	0.35	0.17	0.12	bal

The test specimens for the tensile test were prepared as in Figure 1. Three specimens were obtained from the plate material as a group using wire cutting. The tensile test was performed on these specimens in a WDW-100KN testing machine with a strain rate of 1 mm/min. The mechanical property parameters of 1561 aluminium are shown in Table 2, and the true stress-strain data obtained from the test is plotted as a curve in Figure 2.

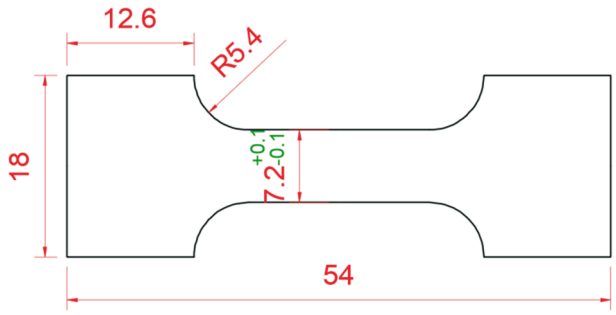

Fig. 1 Tensile test specimen

Table 2 Mechanical property of 1561aluminium

Modulus of elasticity /GPa	Poisson's ratio	Yield strength /MPa	Tensile ratio/%	Fracture strength /MPa	Section shrinkage rate/%
68.365	0.3	216.38	23	498.8	17

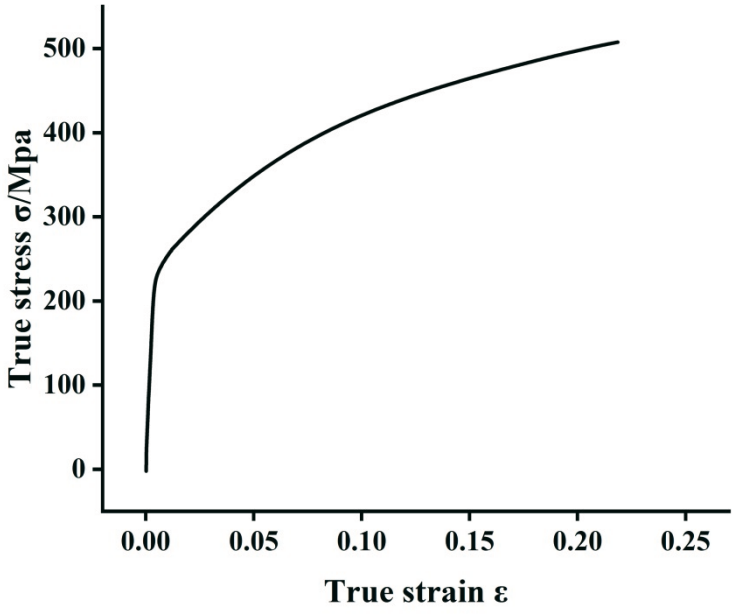

Fig. 2 True stress-strain curve of 1561aluminium alloy

3. Model establishment

3.1 Establishment of the geometric model

As shown in Figure 3, a circular tube with a closed end was drawn using CATIA software. It is a circular tube with a wall thickness of 3 mm obtained from concentric circles of 394 mm and 400 mm in diameter and rotated with a radius of 2250 mm. The double curved part was selected from the above-mentioned circular tube, the length of its ad side and bc side are 2050mm and 2450mm respectively, and the part sheet was obtained by surface unfolding. The diagonal lines ac and bd were used as the inspection lines for the forming accuracy of the part, and their intersection point was set as the coordinate origin O. Next, the right angle coordinate system was established with the width direction of the plate as the X-axis direction, the length direction as the Y-axis direction, and the normal direction of the plate plane as the Z-axis direction.

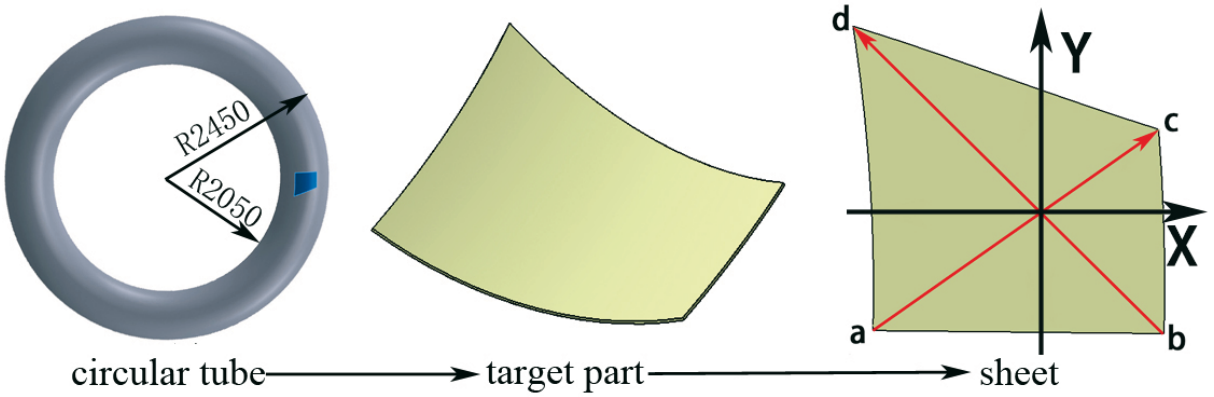

Fig. 3 Sheet required from the target

The modelling of a multi-point die requires calculating the coordinates of each punch P_0 as shown in Figure 4. $P(u\ ,v)$ is the formula for the curve and $P_r(u\ ,v)$ is the formula for the curve containing P_0. The coordinates of the punch centre point P_0 can be calculated by formula (1):

$$\begin{aligned} P(u_s,v_t)+r\mathbf{n}\big|_{x=x_0} &= x_0 \\ P(u_s,v_t)+r\mathbf{n}\big|_{y=y_0} &= y_0 \end{aligned}, \tag{1}$$

where (u_s,v_t) is the tangent point coordinates of the punch and the curve, $\mathbf{n}$ is the tangent plane unit normal vector, and r is the radius of the spherical crown [17].

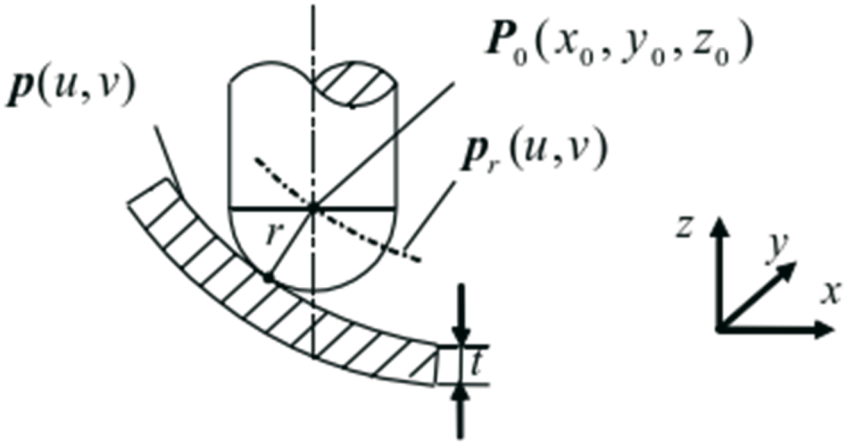

Fig. 4 Touching between punch and part

The forming area of the multi-point forming equipment is 1200 mm×1600 mm, and the maximum forming force that can be applied is 200 kN. Taking the curved part as the target, only the ball crown part of the punch is taken to build the geometric model of the die as shown in Figure 5, the diameter of the ball crown of the punch is 39 mm, and the distance between the adjacent punches is 40 mm.

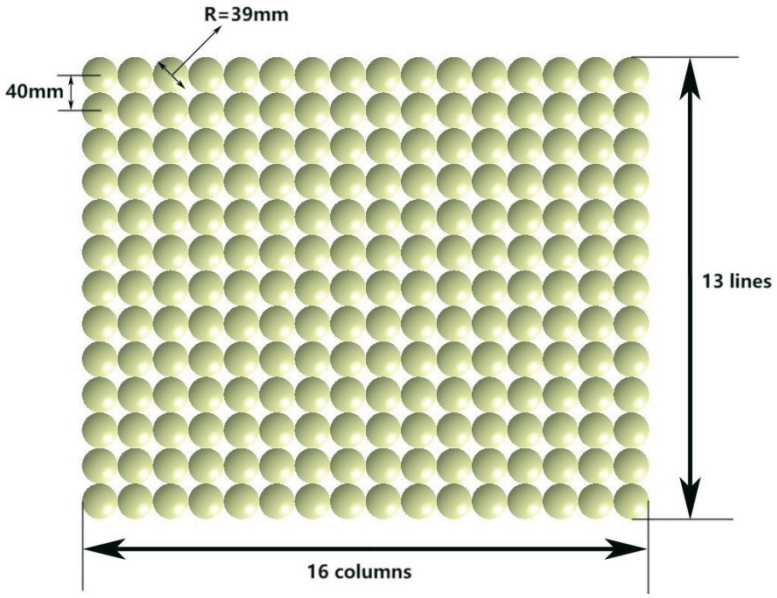

Fig. 5 Geometric model of multi-point die

3.2 Material model

Aluminium alloy adopts VonMise isotropic yield criterion, and its properties are in accordance with the isotropic elastic-plastic constitutive relation [18]. In the finite element calculation, when the obtained increment is small enough, the stress increment and strain increment can be considered to be linear. Only isotropic and hardened elastoplastic metallic materials are considered to represent the strain energy density during deformation, which is a function of the Green strain tensor. The intrinsic model of the material is as follows:

$$\Delta S_{ij} = \frac{\partial^2 W}{\partial E_{ij} \partial E_{kl}} \Delta E_{kl}, \tag{2}$$

where S_{ij} is the Kirchoff stress tensor.

3.3 Finite element calculation method

The dynamic explicit analysis method is used to simulate the stamping process of the plate, which is based on the kinematic formula:

$$\mathrm{M}\ddot{U}(t) + C\dot{U}(t) + F(t) = P(t), \tag{3}$$

where $\ddot{U}(t)$ is the acceleration, M is the mass matrix, $\dot{U}(t)$ is the velocity, C is the damping matrix, $F(t)$ is the internal force vector, and $P(t)$ is the external force vector. In the case of knowing the (0, ..., t_n) time step solution, the central difference time integration method is used to solve the displacement at the moment of t_{n+1} by the formula (4)(5):

$$U(t_{n+1}) = U(t) + \dot{U}(t_{n+1/2})\Delta t_{n+1/2} \tag{4}$$

$$\dot{U}(t_{n+1/2}) = \dot{U}(t_{n-1/2}) + \ddot{U}(t_n)\Delta t_n, \tag{5}$$

where $\Delta t_{n+1/2} = \frac{\Delta t_n + \Delta t_{n+1}}{2}$. The geometric configuration at the moment t_{n+1} can be obtained by updating it at the moment t_n, where $\Delta t_n \le \min\left(\frac{L_e}{c}\right)$, L_e is the minimum cell characteristic size, and c is the wave velocity:

$$c = \sqrt{\frac{E}{(1+\upsilon^2)\rho}}, \tag{6}$$

where E is the modulus of elasticity, υ is the Poisson ratio, and ρ is the density.

The plate and the elastic pad are divided by a C3D8R mesh cell, the cell precision is set to a first order, and the size is 1 mm. The punch is defined as a discrete rigid body cell, and it is divided by a R3D4 mesh cell with a mesh size of 1.1 mm, after the assembly drawing mesh division as in Figure 6.

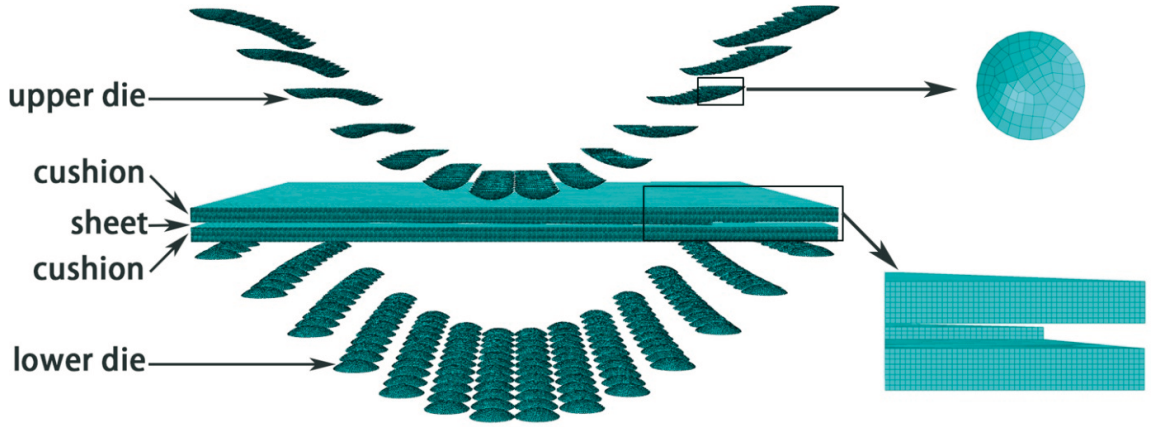

Fig. 6 Finite element meshing of multi-point stamping models

3.4 Simulation condition

The contact force is calculated using the penalty function method, using the Cullen friction model to calculate the tangential force as follows :

$$\tau = \mu\sigma_n \text{ or } P_t = \mu P_n, \tag{7}$$

where μ is the friction coefficient, τ is the friction stress, σ_n is the positive stress, P_t is the friction force, and P_n is the positive pressure. The coefficient of friction between the punch and the elastic pad is 0.15, and the coefficient of friction between the elastic pad and the sheet is 0.2. Fixing the lower die, the upper die moves down to apply the forming force to the sheet, and the pressing process is divided into two dynamic explicit analysis steps [19]: the first analysis step is when the upper die moves down quickly near the part, and the second step decreases the speed to deform the part slowly. When the elastic pad is compressed by 30%, the downward movement is stopped, and the loading is completed.

3.5 Springback calculation

The springback of the formed part is calculated using the static implicit algorithm, and the three points of the formed part are constrained as in Figure 7. Due to the internal stress releasing of the part, it undergoes springback deformation. The motion formula of the node can be expressed as follows:

$$[K]\{X(t+\Delta t)\} = \{F(t+\Delta t)\}, \tag{8}$$

where K is the stiffness matrix, X is the nodal displacement, and F is the nodal force function $\tau = \mu\sigma_n$.

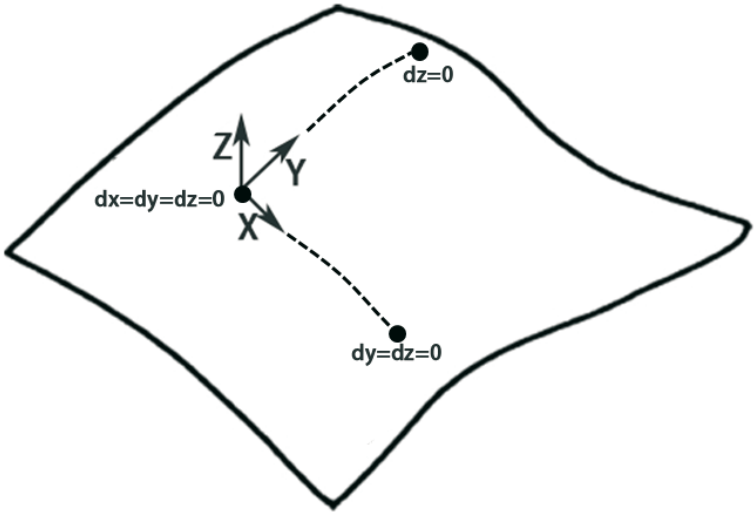

Fig. 7 Constraints on the rebound model

4. Numerical simulation

4.1 Design of curve springback compensation

Figure 8 shows a comparison of the contours of the double curved part before and after the springback of single-step, multi-point forming, where the orange grid shows the contours of the part before the springback. It can be clearly seen that the 1561 aluminium double curved part has severe springback before and after unloading in single multi-point forming which needs to be given large springback compensation. Considering the difference of the hyperbolic parts in different directions of X and Y, different compensation methods are used to apply compensation opposite to the springback direction to the multi-point mould, so that the unloaded surface can be closer to the target shape.

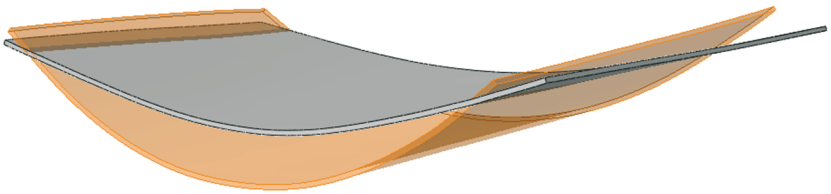

Fig. 8 Springback phenomenon of sheet forming

Since the X-direction radius of the part is relatively small and the Y-direction radius is larger, the amount of springback compensation in the X and Y directions is different. The height Z of any position on the compensation surface is determined by assuming that the height value of any point (x, y) on the target surface part is h, the X-directional contour compensation factor

is m , and the Y-directional contour compensation factor is n , written as $XmYn$. Then, the formula for calculating the amount of springback compensation of the part is as follows [20]:

$$Z=\begin{cases}(1+m)h\ located\ on\ the\ X\ axis\\(1+n)h\ located\ on\ the\ Y\ axis\\(1+m+n)h\ located\ on\ non-cooedinate\ axis\end{cases}. \tag{9}$$

4.2 Optimized design of the forming path

A reasonable deformation path enables the deformed sheet to be uniformly stressed and thus uniformly deformed. Meanwhile, it can reduce the generation of forming defects and achieve parts with better forming results. As the sheet deforms along the ideal forming path, the formula for the Hencky deformation of the sheet at any time t is as follows [21]:

$$U(X,t)=Q(t)Diag[\lambda^{\alpha(t)}(t)]Q^{T}(t), \tag{10}$$

where U is the elongation tensor, X is the node coordinates of intermediate configurations, $Q(t)$ is the orthogonal rotation tensor, $Diag[\lambda^{\alpha(t)}(t)]$ is the diagonal tensor composed of the principal values of *Hencky* strain, $\lambda^{\alpha(t)}(t)$ is the principal value of $U(X,t)$, and $\alpha(t)$ is the deformation parameter.

By establishing the generalized function equation, the deformation of the intermediate configuration is constructed by numerical methods with the least error in the least squares sense. The intermediate configuration is constructed by numerical methods as follows:

$$\begin{aligned}&t_x^{*}=\arg\min\psi({}^{t}x)=\\&\arg\min[\int_{{}^{t}\Omega}\frac{1}{2}(U-\hat{U}):(U-\hat{U})d^{t}\Omega]\end{aligned}, \tag{11}$$

where t_x^{*} is the amount of deformation at x at t moment, ψ is the least squares function, $\hat{U}$ is the deformation tensor of the ideal intermediate configuration calculated by formula (11), U is the deformation tensor of the intermediate configuration calculated by a numerical calculation method, and ${}^{t}\Omega$ is the intermediate configuration at moment t .

The node coordinates of the intermediate configuration unit constructed can be calculated as follows:

$$\begin{aligned}&\frac{\partial\psi(X^{node})}{\partial X^{node}}=\\&\sum_{e}[\int_{{}^{t}\Omega_e}(U-\hat{U})\frac{\partial U}{\partial X^{node}}d^{{}^{t}\Omega_e}]\end{aligned}, \tag{12}$$

where ${}^{t}\Omega_e$ is the volume of the configuration at moment t and X^{node} is the node coordinate of the cell in the initial configuration.

The intermediate configuration at time t can be obtained by solving formula (12). Since the initial and intermediate configurations are designed according to the ideal path, the optimal forming path can be obtained by formula (12). Since the die for multi-step, multi-point forming cannot be changed instantaneously, the multi-step forming path is designed with reference to the most optimal path as shown in Table 3, and the dimensional accuracy of the formed parts obtained with different paths is verified by numerical simulation, and the best multi-step forming path is determined as well.

Table 3 Multi-step forming solution

	First step	Second step	Third step	Fourth step
One step	X2.5Y1.0			
Two steps	X2.2Y1.1	X2.4Y1.2		
Three steps	X1.9Y1.2	X2.1Y1.3	X2.3Y1.4	
Four steps	X1.7Y1.3	X1.9Y1.4	X2.1Y1.5	X2.2Y1.5

4.3 Analysis of the numerical simulation results of different paths

The simulation results are shown in Figure 9. The parts formed by one, two, and three steps, respectively, show different degrees of wrinkling, and the wrinkling is gradually reduced as the number of steps increases. It is clear that the surface quality of the part formed in four steps is quite good.

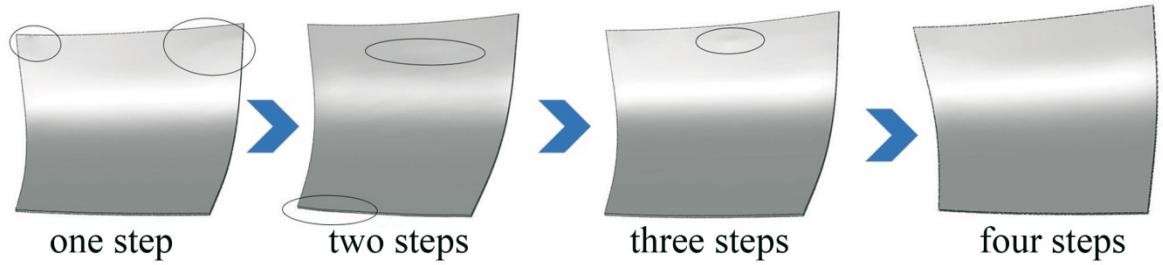

Fig. 9 Surface wrinkling of forming parts

As shown in Figure 10, compared to single-step forming, four-step forming results in a more uniform force on the double curved part. As well as having a larger area for the plastic deformation of the material as it reaches yield conditions, it allows for more suitable force on the edges of the part, and is helpful for forming the edge locations of the curved parts.

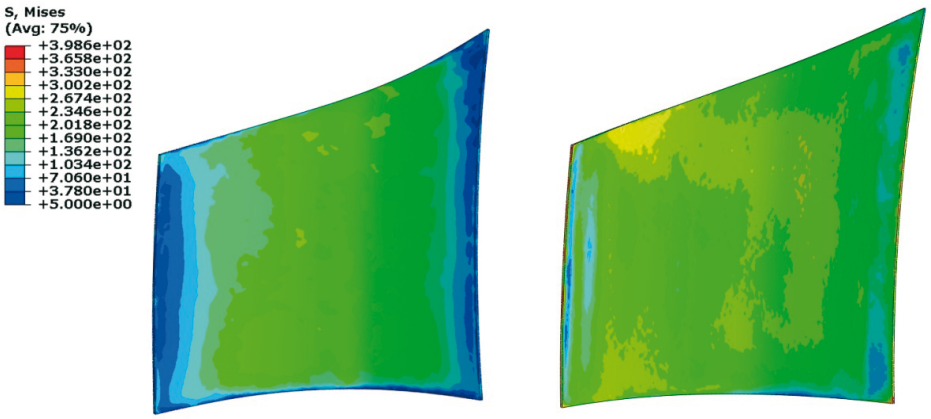

a: single-step forming part b: four-step forming part

Fig. 10 Von Mises stress distribution nephogram

After deformation of the curved part, the position of the four vertices is shifted. In order to obtain a more accurate outline of the part, set point a and b as the origin of the coordinate axis, respectively. Set ac and bd as the positive direction of the x-axis, and the normal direction of the plane as the z-axis to establish the coordinate system. An outline of the part is drawn out as in Figure 11. With the increasing number of forming steps, the inspection line contour gradually approximates the target part contour, and, at the same time, the dimensional accuracy gradually improves.

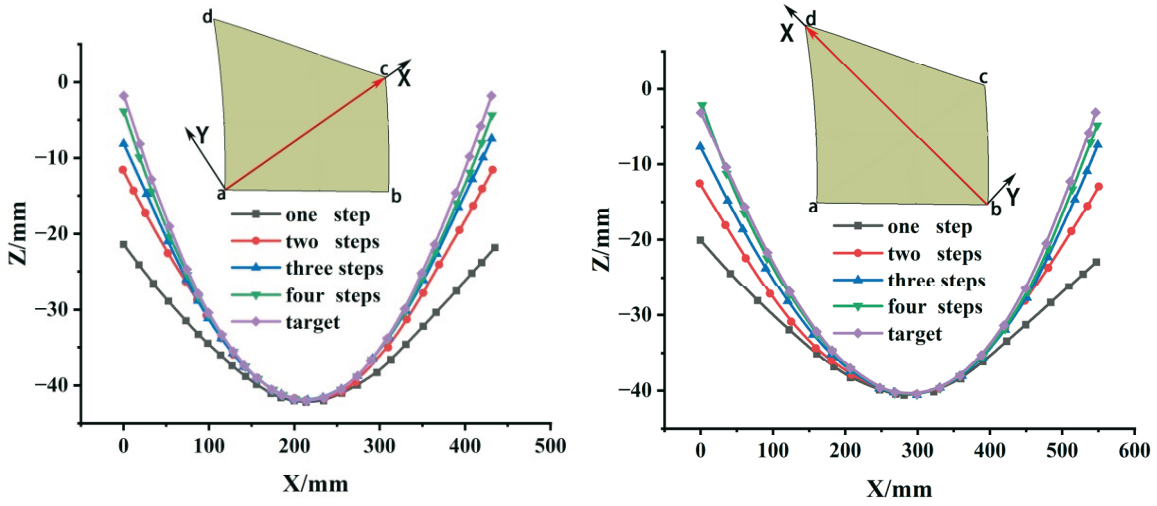

a: profile outline of ac

b: profile outline of bd

Fig. 11 Part dimensions in different paths

The maximum errors of the four formed parts on the ac and bd paths were taken and the relation between the maximum errors and the number of forming steps was plotted in Fig. 12. Compared with single-step forming, the maximum errors of the four formed parts on the ac and bd paths were reduced by 85% and 80%, respectively.

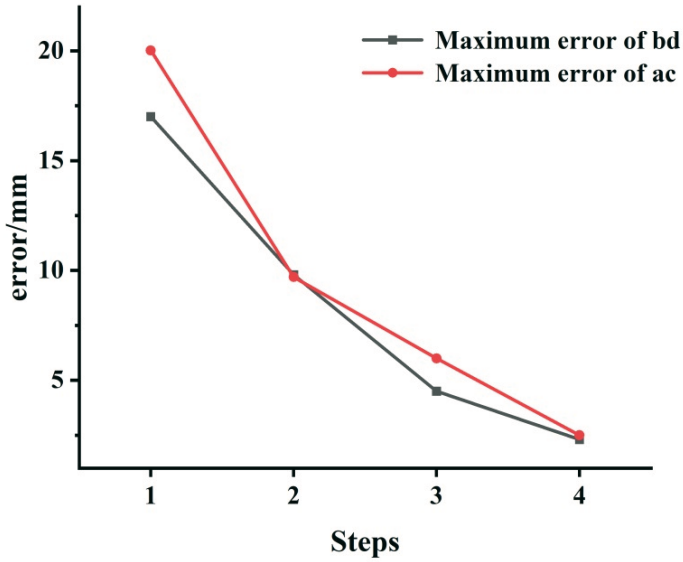

Fig. 12 Variation of the maximum error with forming times

4.4 Four-step multi-point forming analysis

Figure 14 shows the contour lines in the ac and bd directions of the part formed in four steps. By increasing the number of forming steps, the curvature of the part profile is increased, which improves the problem of part edge forming and gradually improves the forming accuracy of the part. This is because the edge of the curved part has a bending moment M opposite the bending direction during the multi-point forming process, as shown in Figure 13.

$$M = F_2 L_2 \tag{13}$$

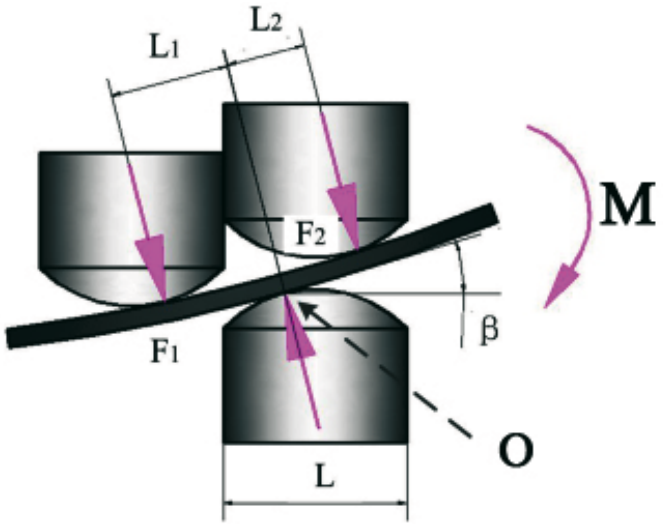

Fig. 13 The state of the force at the edge of the part

The larger springback compensation increases the tangential angle β between the curve and the punch, which increases the length of L_2 and the magnitude of the bending moment M. Multi-step forming results in a smaller part of deformation and a reduced angle β, which allows the bending moment M in the opposite direction of the part to be reduced, making it easier for the edges of the part to be formed.

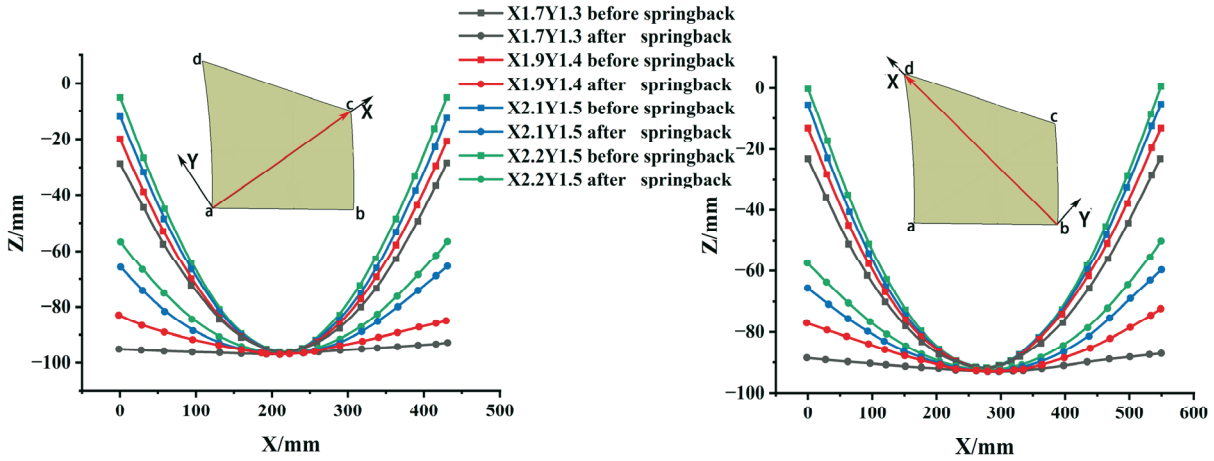

a: profile outline of ac

b: profile outline of bd

Fig. 14 Part dimensions in different steps

5. Experimental

The double curved plate made of 1561 aluminium alloy is stamped with four multi-point forming steps, and the dimensions of the resulting plate and basic body are the same as those of the numerical simulation. Figure 15 shows photographs of the multi-point stamping machine and the experimental parts.

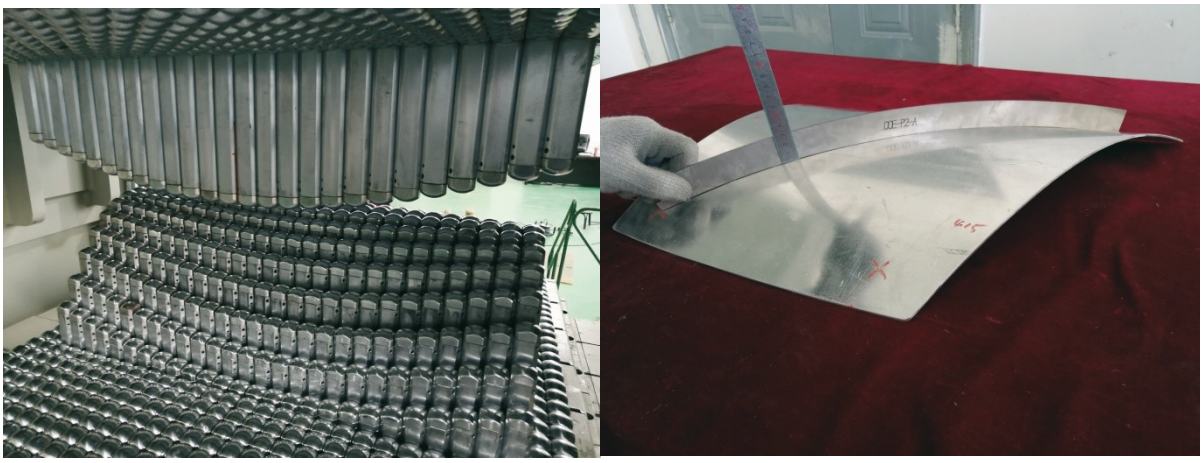

a: multi-point forming stamping machine b: the formed part

Fig. 15 Multi-point stamping machine and the formed part

The optical scanning of the four-step forming part by Scan 3D scanner was used to obtain the point cloud data of the forming part surface. The point cloud data of the formed part are converted into a geometric model by Gom-inspect analysis software. The geometric model that is converted from the point cloud data of the formed part by Gom-inspect analysis software is compared with the dimensions of the target part, and the error distribution of the formed part is produced as shown in Figure 16. It can be seen that the error is maximum at point a, which is 2.6 mm. The rest of the error is small.

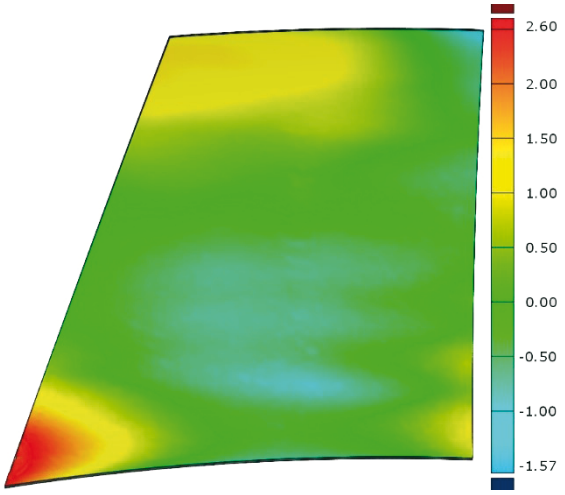

Fig. 16 Shape error cloud of the formed part

As shown in Figure 17, for the error distribution of the formed parts, 91.7% of the areas in the Figure show dimensional errors less than 1 mm, and only 0.8% of them exceed 2 mm, which indicates that the simulation results fit well with the actual situation. In the multi-point forming of double curved parts of 1561 aluminium alloys, it is possible to obtain parts with small dimensional errors by using the four-step forming path along X1.7Y1.3, X1.9Y1.4, X2.1Y1.5 and X2.2Y1.5 as shown in this paper. The error of the formed part meets the requirements with a maximum error of 3 mm.

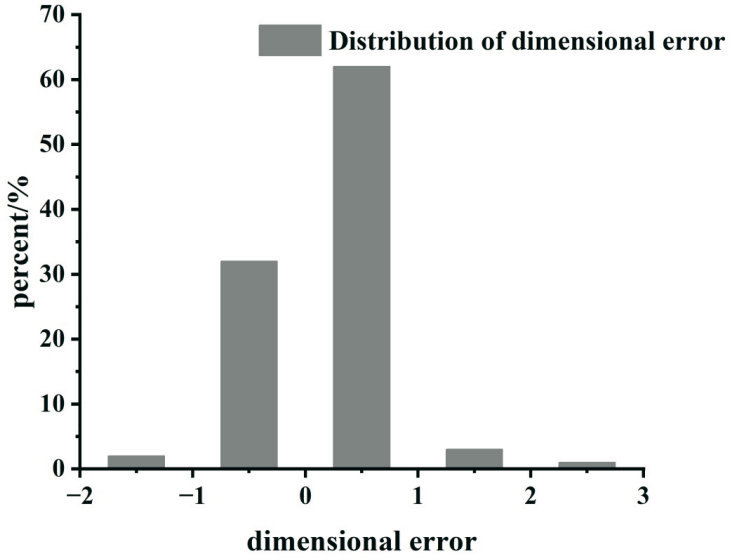

Fig. 17 Shape error distribution of the formed work part

6. Conclusion

(1) The dynamic explicit algorithm of the finite element analysis method was used to simulate the loading and forming process of 1561 aluminium alloy. Then, combined with the static implicit algorithm, the unloading springback process was simulated numerically. According to the calculations, it was found that the 1561 aluminium alloy has severe springback, and large springback compensation is needed during the forming process. Wrinkling happens with single-step multi-point forming.

(2) For the 1561 aluminium alloy double curved part, adopting a four-step forming path can avoid surface wrinkling, reduce part errors, and improve the forming quality of part edges. The better forming paths are X1.7Y1.3, X1.9Y1.4, X2.1Y1.5, X2.2Y1.5.

(3) The results of the simulation were verified and fit well with the experimental results, which can serve as guidance for actual production.

REFERENCES

[1] D. Loganathan et al. “Grey relational analysis-based optimisation of input parameters of incremental forming process applied to the AA6061 alloy”. Transactions of FAMENA, 2020, 44(1): 93-104. https://doi.org/10.21278/TOF.44108

[2] M. Li et al. “Multi-point forming: a flexible manufacturing method for a 3d surface sheet”. Journal of Materials Processing Tech, 1999, 87(1) : 277-280. https://doi.org/10.1016/S0924-0136(98)00364-1

[3] Subramani et al. “Studies on testing and modelling of formability in aluminium alloy sheet forming”. Transactions of FAMENA, 2018, 42(2): 67-80. https://doi.org/10.21278/TOF.42206

[4] T. Yue et al. “A springback prediction method for double-curved plate bent with the multi-point forming method proceedings of the institution of mechanical engineers”. Journal of Aerospace Engineering, 2020, 234(12): 1939-1952. https://doi.org/10.1177/0954410020921313

[5] Q. Zhang et al. “Compensation algorithm for springback in multi-point forming and its validation”. Journal of Jilin University (Engineering and Technology Edition), 2012, 42(06): 1448-1452.

[6] Z. Qian et al. “Numerical simulation study on the process of multi-point press forming and multi-step multi-point die forming”. Journal of Plasticity Engineering, 2007(03): 20-23.

[7] W. Fu et al. “Multi-point forming process of 1561 aluminum alloy surfaces”. Journal of Jilin University (Engineering and Technology Edition) , 2017, 47(06): 1822-1828.

[8] L. Zhang. “Research on shape precision control of curved parts in multi-point forming”. College of Materials Science and Engineering, Jilin University, 2019.

[9] G. Sun et al. “Influence of different technology modes on spring-back in multi-point forming”. Journal of University (Engineering and Technology Edition), 2006, (3): 274-278.

[10] S. Wang et al. “Numerical simulation analysis on the influence factors of springback in multi-point stretch forming”. Journal of Plasticity Engineering, 2009, 16(04): 7-11.

[11] C. Liu et al. “Springback prediction method for double-curved workpiece considering plate anisotropy in multi-point forming”. Journal of Mechanical Science and Technology, 2021, 35(6): 2623-2636. https://doi.org/10.1007/s12206-021-0533-0

[12] Z. Qian et al. “Numerical simulation on the process of sphere surface multi-step multi-point forming”. Journal of Jilin University (Engineering and Technology Edition), 2007, (2): 338-342.

[13] I. Uzelac et al. “A new algorithm for dynamic analysis of thin plates in the combined finite-discrete element method”. Transactions of FAMENA, 2015, 39(2): 47-54.

[14] R. Hao et al. “The study on numerical simulation of multi-steps of multi-point forming”. Journal of Plasticity Engineering, 2006, (1): 18-21.

[15] Q. Zhang et al. “Study on springback compensation in multi-point forming”. Manufacturing Process Technology, Pts 1-5, 2011, 189-193: 2957-2960. https://doi.org/10.4028/www.scientific.net/AMR.189-193.2957

[16] W. Liu et al. “Numerical simulation on the process of saddle surface multi-step multipoint die forming”. Machinery Design & Manufacture, 2009(02): 242-244.

[17] H. Peng et al. “Numerical simulation of multi-point forming accuracy for polycarbonate sheet”. Proceedings of the Institution of Mechanical Engineers, Part E: Journal of Process Mechanical Engineering, 2014, 228(2) : 87-96. https://doi.org/10.1177/0954408913475562

[18] M. Predrag et al. “Isogeometric FEM analysis of complex thin-walled structures”. Transactions of FAMENA, 2015, 39(1): 15-26.

[19] Ahmed et al. “Techniques for mesh independent displacement recovery in elastic finite element solutions”. Transactions of FAMENA, 2021, 45(2): 41-58. https://doi.org/10.21278/TOF.452019720

[20] Z. Xiong et al. “A study on the explicit expression of critical stress and Euler stress and its application”. Transactions of FAMENA, 2019, 43(1): 15-28. https://doi.org/10.21278/TOF.43102

[21] E. Qu. “Research on formability in multi-point forming with different elastic pads”. The International Journal of Advanced Manufacturing Technology, 2018, 98(5-8): 1887-1901. https://doi.org/10.1007/s00170-018-2192-6

Submitted: 14.11.2022

Accepted: 21.3.2023

Zhongfeng Zhang
Dieless Forming Technology Center, Jilin University, Changchun, China
Qingwen Xue
Lixia Wen
Weihua Peng
Cssc HuangPuWenchong Shipbuilding Company Limited, Guangzhou, China
Han Shao
Wenzhi Fu*
Dieless Forming Technology Center, Jilin University, Changchun, China
*Corresponding author:
fwz@jlu.edu.cn